SURFACE CAPACITY OF ELECTRICALLY SYNCYTIAL TISSUES

DAVID N. LEVIN, *Departments of Medicine and the Pharmacological and Physiological Sciences, University of Chicago, Chicago, Illinois 60637*

ABSTRACT An exact geometry-independent formula is derived that gives the total surface membrane capacity of an electrical syncytium in terms of its input resistance (R_{IN}) and the phase angle (ϕ) of its complex admittance. The formula strips off the effects of resistance in the extracellular space and exposes the true capacity of the external surface of preparations such as skeletal muscle fibers, cardiac Purkinje fibers, or spherical cardiac aggregates. The shape, extent, and resistivity of the extracellular space may be arbitrary and need not be measured. The medium in this space may have an arbitrary and nonuniform resistivity. It is assumed that the tissue is impaled with current and voltage electrodes, so that the intracellular resistance between the electrodes and membranes is negligible or can be dealt with by theoretical calculations. Under these circumstances the total surface membrane capacity at high frequency is determined exactly by R_{IN} and a frequency domain integral over ϕ. The method is tested with synthetic data for R_{IN} and ϕ generated by the "disk" model of skeletal muscle fibers and the "pie" model of cardiac Purkinje fibers. The formula allows the "inversion" of these data and the deduction of the correct value of the total surface membrane capacity.

I. INTRODUCTION

Impedance locus measurements on single uninvaginated cells directly reflect the membrane characteristics of the naked membrane. The membranes of invaginated cells (e.g., skeletal muscle) or multicellular preparations (e.g., cardiac tissue) are electrically obscured by the effects of intra-cellular and extracellular resistance. The effects of intracellular resistance can be removed by preparing small tissue samples, by applying the three-microelectrode technique (Adrian et al., 1970), or by calculation (Eisenberg and Johnson, 1970). This paper addresses the more serious problem of extra-cellular resistance. The most straightforward method of dealing with this problem is to adopt a detailed model of size, shape, and specific resistivity of the extracellular space. The characteristics of the unit membranes can then be deduced by removing the calculated effects of extracellular resistance from the electrical measurements on the tissue. For example, skeletal muscle fibers have been analyzed in this way with the aid of the disk and mesh models of the T system (Falk and Fatt, 1964; Adrian et al., 1969; Mathias et al., 1977). A theoretical treatment applicable to aggregates of large numbers of small cells is described in the syncytial theories of Eisenberg et al. (1979) and Peskoff (1979). Data from sheep cardiac Purkinje fibers have been interpreted in the context of a variety of models that contain between 6 and 54 cells in transverse section (Levin and Fozzard, 1981). Modeling of this kind has the disadvantage of being both laborious and inaccurate. The theoretical accuracy of this approach is limited because a mathematically tractable model will only approximate the complicated geometry of a real tissue. For example, Levin and Fozzard

(1981) have shown how the unit membrane conductance and capacitance that are inferred from Purkinje fiber data depend upon whether the fiber is modeled as a cell aggregate with three or six cells meeting at each intercellular junction.

In this paper and the following one we derive geometry-independent formulas that express unit membrane parameters in terms of electrical measurements on the whole preparation; it is not necessary to measure or model the geometry or resistivity of the extracellular space. The method is best illustrated by considering the measurement of the total capacity of a preparation's surface membrane (i.e., the membrane facing the bath). We know that membranes behave as capacitors at high frequency. Since the invaginated membrane (i.e., the membrane facing the extracellular space) is in series with some fraction of the extracellular resistance, a high-frequency current will flow preferentially through the surface membrane of the preparation. Therefore, at sufficiently high frequency the magnitude of the impedance of the whole preparation will be the inverse of the product of the surface capacity and angular frequency. In principle, this means that total surface membrane capacity can be obtained by making high-frequency impedance measurements. In practice, this is not possible since technical problems make it difficult to measure the magnitude of the impedance in the desired frequency range (well above 5,000 Hz in skeletal muscle and Purkinje fibers). This problem can be circumvented in the following way. Impedance locus measurements determine the magnitude and phase angle of the complex impedance of the preparation at each frequency. As long as the fiber is in a state that is stable under electrical perturbations, it is possible to show that its complex impedance is an analytic function in the complex frequency plane. It follows that some of the impedance locus data is redundant; specifically, it is possible to derive a generalization of the Kramers-Kronig relation (Kronig, 1926; Cole and Cole, 1941) that gives the magnitude of the complex impedance at any frequency in terms of the surface capacity and a frequency domain integral over the phase angle of the impedance ($-\phi$). Because the input resistance (R_{IN}) is just the magnitude of the complex impedance at zero frequency, the surface membrane capacity can be expressed in terms of R_{IN} and an integral over ϕ. In most cases this integral is dominated by low frequency values of the phase angle; therefore, the total surface capacity of the tissue can be deduced accurately from relatively low-frequency electrical measurements. Changes in the size, shape, or resistivity of the extracellular space cancel out when R_{IN} and ϕ are substituted into the formula, and the calculated value of surface membrane capacity is unaffected. In other words, the formula gives the surface capacity as an invariant, geometry-independent combination of electrical measurements on the preparation.

It is not possible to use the tissue impedance locus to deduce the magnitude of membrane resistivity without modeling the geometry and resistivity of the extracellular space. However, in many cases the actual magnitude of membrane resistivity or capacitance is not particularly interesting; often it is more important to know what *changes* in these parameters are caused by an intervention (e.g., addition of a channel-blocking agent to the bath or a change in the membrane holding potential). In the following paper (Levin, 1981) geometry-independent formulas are given for inferring the changes in invaginated and surface membrane resistivity and capacitance from the changes in phase angle and input resistance induced by such an intervention.

II. FORMULA FOR EXTERNAL SURFACE MEMBRANE CAPACITY

This section contains the statement and discussion of the formula for external surface capacity. The mathematical details of the proof are given in Appendix A.

The following is a list of the assumptions that lead to the formula:

1) The tissue preparation is assumed to have a smooth external surface with total area S_e. The extracellular space may have any size and shape; it is connected to the bath by well-defined mouths.

2) The medium in the extracellular space is assumed to be purely resistive. Its specific resistivity can be spatially inhomogeneous.

3) The external surface (invaginated) membrane is assumed to have the high-frequency behavior of a capacitor with average specific capacitance C_{me} (C_{mi}). Each patch of membrane may be characterized by an otherwise arbitrary linear electrical circuit that may vary from place to place in the tissue preparation. For example, the electrical circuit in any patch may be an RC circuit supplemented by the additional inductive and capacitive limbs that appear in a linearized Hodgkin-Huxley-type model (Cole, 1972).

4) The tissue is assumed to be impaled with current and voltage electrodes in such a way that the effects of intracellular resistance are negligible or can be dealt with theoretically; i.e., the voltage within the intracellular space is assumed to be spatially uniform across the whole preparation.

5) The preparation is assumed to be stable to electrical perturbations. This means that

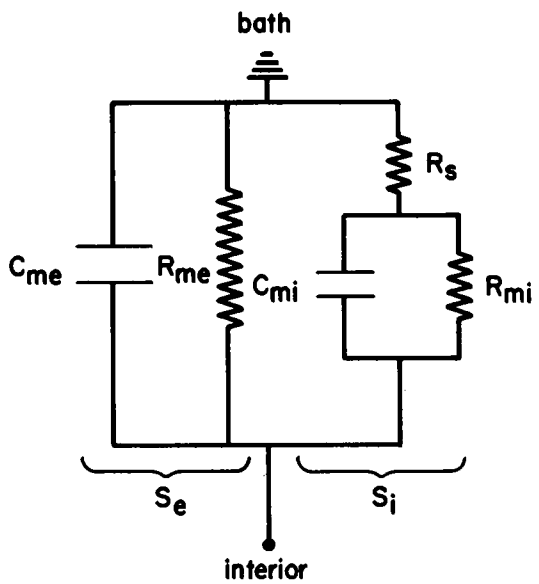

FIGURE 1 This is the simplest "lumped" circuit which might represent a preparation with surface (invaginated) membrane area $S_e(S_i)$. C_{me} and R_{me} (C_{mi} and R_{mi}) denote the specific capacitance and resistivity of the unit surface (invaginated) membrane. The effect of extracellular space is represented crudely by the series resistor R_S.

small steps in voltage (current) lead to small steady steps in current (voltage) after transients have disappeared.

In Appendix A it is shown that these assumptions lead to the following formula for $S_e C_{me}$, the total external surface membrane capacity:

$$S_e C_{me} = \frac{\tau_H}{R_{IN}\Gamma(0)}, \tag{1}$$

where:

$$\Gamma(0) = \exp\left\{\frac{2}{\pi}\int_0^\infty \frac{d\omega}{\omega}\left[\tan^{-1}(\tau_H\omega) - \phi\right]\right\}.$$

In the above equations R_{IN} is the input resistance of the preparation. $\phi(\omega)$ is the phase angle of the preparation's admittance at angular frequency ω; i.e., it is the phase lag between the voltage and the driving current at frequency $\nu = \omega/2\pi$. τ_H is an arbitrary positive number that serves to make the integral converge but that cancels out exactly in the overall expression for $S_e C_{me}$. Notice that the factor ω, which appears in the denominator of the integral, will cause the integral to be insensitive to errors in the phase angle measurements at high frequency.

Eq. 1 allows the "inversion" of the phase angle data and the extraction of the total surface membrane capacity. This procedure is valid no matter what electrical circuit represents the behavior of the whole tissue. It is instructive to verify this result for a simple circuit in which the integral can be done analytically. Consider the "lumped" circuit in Fig. 1 for the special case in which $R_{me} = R_{mi} = R_m$ and $C_{me} = C_{mi} = C_m$. Direct computation of the admittance of this circuit shows that its phase angle is

$$\phi = \tan^{-1}(R_m C_m \omega) + \tan^{-1}\left(\frac{c\omega}{a + b\omega^2}\right), \tag{2}$$

where

$$a = \left(1 + \frac{R_s}{R_m}\right)\left(1 + \frac{R_s}{R_m} + \frac{S_i}{S_e}\right),$$

$$b = (R_s C_m)^2,$$

$$c = -\frac{S_i}{S_e} R_s C_m.$$

The input resistance is

$$R_{IN} = R_m\left(S_e + \frac{S_i R_m}{R_s + R_m}\right)^{-1}. \tag{3}$$

I want to substitute these expressions into the right-hand side of Eq. 1 and verify that the result is just $S_e C_m$. The exponent in $\Gamma(0)$ can be broken into two terms:

$$\Gamma(0) = e^I e^{II}, \tag{4}$$

where

$$I = \frac{2}{\pi}\int_0^\infty \frac{d\omega}{\omega}\left[\tan^{-1}(R_m C_m \omega) - \phi\right]$$

$$= -\frac{2}{\pi}\int_0^\infty \frac{d\omega}{\omega}\tan^{-1}\left(\frac{c\omega}{a + b\omega^2}\right)$$

$$II = \frac{2}{\pi}\int_0^\infty \frac{d\omega}{\omega}\left[\tan^{-1}(\tau_H \omega) - \tan^{-1}(R_m C_m \omega)\right].$$

I can be evaluated by differentiating it with respect to a and finding the resulting integral in a table (Dwight, 1962):

$$\frac{dI}{da} = \frac{2c}{\pi}\int_0^\infty \frac{d\omega}{b^2\omega^4 + (2ab + c^2)\omega^2 + a^2}$$

$$= \frac{c}{a\sqrt{4ab + c^2}}.$$

Now both sides can be integrated from a to ∞ (where $I = 0$) with the result

$$I = \ln\left|\frac{\sqrt{4ab + c^2} - c}{\sqrt{4ab + c^2} + c}\right|.$$

Substituting the values of a, b, and c (Eq. 2) into the right-hand side gives

$$I = \ln\left[1 + \frac{S_i R_m}{S_e(R_s + R_m)}\right]$$

and

$$e^I = 1 + \frac{S_i R_m}{S_e(R_s + R_m)}. \tag{5}$$

II can be evaluated by noting that its derivative with respect to τ_H gives a tabulated integral (Dwight, 1962):

$$\frac{dII}{d\tau_H} = \frac{2}{\pi}\int_0^\infty \frac{d\omega}{1 + (\tau_H \omega)^2} = \frac{1}{\tau_H}.$$

Integrating both sides between τ_H and $R_m C_m$ (where $II = 0$) gives

$$II = \ln\left(\frac{\tau_H}{R_m C_m}\right)$$

and

$$e^{II} = \frac{\tau_H}{R_m C_m}. \tag{6}$$

Therefore,

$$\Gamma(0) = \frac{\tau_H}{R_m C_m}\left[1 + \frac{S_i R_m}{S_e(R_s + R_m)}\right]. \tag{7}$$

Substitution of Eqs. 7 and 3 shows that the right-hand side of Eq. 1 is equal to $S_e C_m$ as expected; all references to S_i, R_s, and R_m have cancelled out. This calculation illustrates the model-independence of the method; the various electrical and geometric parameters of the extracellular space (such as R_s and S_i) can influence the data for R_{IN} and ϕ separately without affecting the combination of R_{IN} and ϕ used to calculate $S_e C_{me}$. This example also demonstrates the τ_H-independence of the right side of Eq. 1.

A generalization of Eq. 1 is proved in Appendix A. In particular, it is noted that there is great freedom in the choice of the convergence factor in Eq. 1. For example, the term $\tan^{-1}(\tau_H \omega)$ under the integral can be replaced by the phase of any function of frequency with suitable analyticity properties provided that the the τ_H factor in the numerator is replaced by the inverse of the zero frequency limit of that function.

III. APPLICATIONS

This section contains a discussion of the data analysis required to use Eq. 1. The procedure is illustrated by applying it to synthetic data which is generated by the disk model of a skeletal muscle fiber and the pie model of a Purkinje fiber. Finally, I list the sources of experimental error that might be encountered in the use of Eq. 1.

A. *Data Analysis Procedure*

There are five steps in the application of Eq. 1:

1) ϕ must be measured over the widest possible frequency range (denoted by $\nu_0 \leq \nu \leq \nu_M$) under conditions which minimize the effects of intracellular resistance. R_{IN} must also be measured accurately.

2) The data for ϕ must be smoothly extrapolated into lower ($0 \leq \nu \leq \nu_0$) and higher ($\nu_M \leq \nu < \infty$) frequency domains.

3) A convenient value of τ_H is chosen.

4) $S_e C_{me}$ is calculated by having a computer do the integration on the right side of Eq. 1.

5) If the magnitude of C_{me} is needed, the total external surface area (S_e) must be measured.

Intracellular resistance can be reduced in the usual ways. For example, the tissue may be prepared to be physically small (e.g., a spherical aggregate of cardiac cells) or electrically small (e.g., a short length of skeletal muscle or Purkinje fiber under three-microelectrode voltage clamp [Adrian et al., 1970]). In this case R_{IN} and ϕ can be measured directly. If the tissue is not small but has a simple geometry, the effects of intracellular resistance can be removed by calculation (Eisenberg and Johnson, 1970). For instance, consider a long (semi-infinite) cardiac Purkinje strand or a skeletal muscle fiber. If the current and voltage electrodes are separated longitudinally by a distance x, which is greater than one fiber diameter, three-dimensional effects associated with the diverging current flow are insignificant (Eisenberg and Johnson, 1970). Furthermore, it is not difficult to show that the

transverse intracellular resistance is insignificant, since the voltage drop across it is <5% of the voltage drop across the membrane at frequencies up to 10 kHz (Levin and Fozzard, 1981). Therefore, the current flow beyond point x is governed by a cable equation involving longitudinal intracellular resistance and an effective admittance across the membrane and extracellular space. The phase angle (Θ_x) of the transfer admittance and the magnitude of the transfer impedance (Z_x) at electrode separation x are given by the standard cable relations

$$\Theta_x = \Theta_0 + \frac{x r_i \sin \Theta_0}{Z_0}$$

$$\ln Z_x = \ln Z_0 - \frac{x r_i \cos \Theta_0}{Z_0}. \tag{8}$$

Here, r_i is the intracellular resistance of a unit length and can be calculated in the usual way from measurements of the input resistance (R_0) and the DC length constant (Λ) of the whole cable: $r_i = R_0/\Lambda$. Θ_0 and Z_0 are the phase angle and impedance which would be measured at $x = 0$ if there were no three-dimensional effects. Since Θ_x, Z_x, x, and r_i are measurable at each frequency, Eq. 8 constitutes two equations which can be solved for Θ_0 and Z_0 at each frequency. These values can be used to calculate the input resistance (R_{IN}) and phase angle (ϕ) of a unit length of idealized fiber in which there is no intracellular resistance whatsoever: $R_{IN} = \Lambda R_0$, $\phi = 2\Theta_0$. Eq. 1 can then be used to calculate the total surface membrane capacity of a unit length of fiber. This procedure breaks down above 10 kHz when transverse intracellular resistance becomes more than a few percent of the membrane impedance. When this frequency is reached, ϕ will begin to decline instead of continuing its climb to 90°. Therefore, a smooth extrapolation to 90° of the lower frequency behavior of ϕ should remove the effects of transverse intracellular resistance.

With modern techniques (Mathias et al., 1979) it only takes a few minutes to measure ϕ over a wide frequency range (e.g., above ν_0 = 1 Hz and below ν_M = 5,000 Hz). Since the frequencies at which ϕ is measured can be closely spaced, it is easy to interpolate between points during the integration in Eq. 1. At frequencies >5,000 Hz the phase angle can be obtained by smoothly extrapolating its measured behavior in the region just below 5,000 Hz. Models can provide guidelines for choosing a convenient function of frequency for this purpose. For example, models like the disk model of skeletal muscle or the pie model of a Purkinje fiber predict a phase angle with the high frequency behavior:

$$\phi = \frac{\pi}{2} - \frac{1}{(1 + B\nu^{1/2})}. \tag{9}$$

B is a number which depends on the geometry of the tubule or cleft mouths. Physically, Eq. 9 represents the phase angle at a frequency which is so high that most of the current in the extracellular space enters that space through invaginated membrane located near tubule or cleft mouths; little current flows through the more deeply invaginated membrane. For the purpose of the data analysis described here, Eq. 9 can be regarded as a phenomenological form with one free parameter (B), which will give a good fit to the high frequency phase angle data. An example of this high-frequency extrapolation procedure is illustrated by the dashed continuation of the dot-dashed "data" curve in Fig. 2. The surface membrane capacity, which

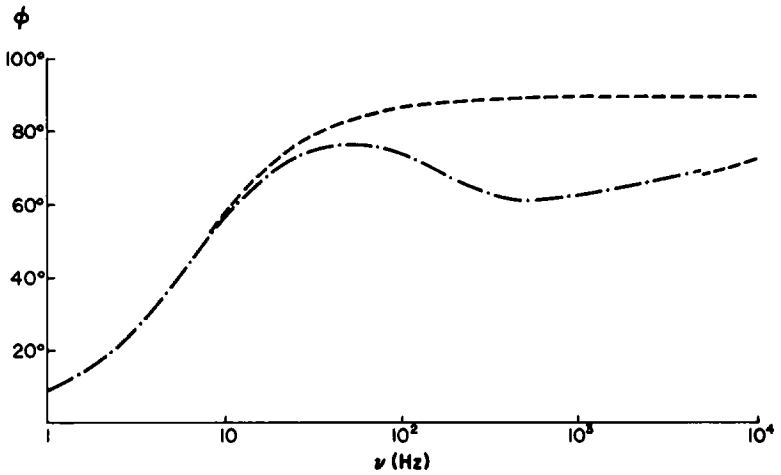

FIGURE 2 The dot-dashed line shows the synthetic data for the phase angle (ϕ) of the admittance of the skeletal muscle disk model. The data are generated when the electrical parameters of the model are given realistic values (shown in the first line of Table I). The lower dashed curve, found by evaluating Eqs. B7 *a* and *b*, represents the behavior of the disk model as $\nu \to \infty$. The upper dashed line is obtained by fitting the function in Eq. 10 to the low-frequency end of the dot-dashed line.

is calculated with the aid of extrapolation of ϕ to high frequencies (say, beyond 5,000 Hz), is a measure of the membrane capacity which is not "lost" at 5,000 Hz. It includes the true loss-free capacity (ideally observed at ∞ frequency) plus the capacity due to processes (e.g., dielectric charge movements) with time constants less than $1/[2\pi(5{,}000)]$ s $\approx 1/30$ ms (Almers, 1978).

The phase angle below ν_0 (e.g., 1 Hz) can be obtained by smoothly extrapolating its measured behavior just above ν_0. The assumption is that there are no important processes with time constants greater than $1/2\pi$ s $\approx$ 160 ms. In most cases, the phase angle just above 1 Hz is well represented by the function

$$\phi = \tan^{-1}(\tau_\phi \omega), \tag{10}$$

where τ_ϕ is chosen to give the best fit. Intuitively, Eq. 10 represents the phase angle at a frequency which is so low that the preparation appears to be uninvaginated; the value of the effective time constant τ_ϕ lies between the values of the surface and invaginated membrane time constants ($R_{mc}C_{mc}$ and $R_{mi}C_{mi}$, respectively). The upper dashed line in Fig. 2 is an example of a curve obtained by fitting τ_ϕ to the low-frequency behavior of the dot-dashed "data" curve.

B. *Skeletal Muscle "Data"*

I now consider the use of Eq. 1 to calculate the total surface membrane capacity of a skeletal muscle fiber. The data analysis is best illustrated by using "synthetic data" generated by the disk model of a skeletal muscle fiber, first proposed by Falk and Fatt (1964) and Adrian et al. (1969). The main features of this model are outlined in Appendix B; more details can be found in Levin and Fozzard (1981), as well as in the original papers. At this point it suffices to say that the values of the model's geometric parameters (see Appendix B) are taken from the

morphometric work of Mobley and Eisenberg (1975). The model is characterized by the following electrical parameters: the specific capacitance (C_{me}) and conductance (g_{me}) of the unit external surface membrane, the specific capacitance (C_{mi}) and conductance (g_{mi}) of the unit invaginated (T tubule) membrane, and the specific resistivity (R_e) of the medium in the T system. The dot-dashed line in Fig. 2 represents the phase angle of the complex admittance of a unit length of this model with a realistic set of membrane parameters (listed in line 1 of Table I) and with no intracellular resistance (see section III A). The input resistance of a 1-mm length of this model is R_{IN} = 1.88 MΩ when intracellular resistance is zero. I now treat these values of ϕ and R_{IN} as "data" to be analyzed as indicated in the previous subsection. In Appendix B a short length of the disk model is shown to be exactly equivalent to the distributed circuit in Fig. 3. Therefore, one is asking if one can use Eq. 1 to calculate the C_{me} of this circuit from knowledge of its input resistance and phase angle. Above 5,000 Hz ϕ is taken to be described by Eq. 9 with a value for B found by evaluating Eq. B7 *b* with realistic disk model parameters, namely, B = 0.0232 $s^{1/2}$; this gives the dashed continuation of the dot-dashed curve in Fig. 2. Although the expression for B in Eq. B7 *b* describes the exact behavior of the disk model as $\nu \rightarrow \infty$, it is not an exact description at 5,000 Hz. This accounts for the slight notch between the low-frequency and high-frequency limbs of the curve in Fig. 2. In an experimental situation, B could be adjusted empirically so that the high-frequency curve smoothly joined the experimental points below 5,000 Hz. Below 1 Hz, ϕ is taken to be described by Eq. 10 with τ_ϕ = 24.9 ms. This value was chosen by equating τ_ϕ with $1/2\pi\, d\phi/d\nu$ at 1 Hz and leads to a low-frequency form of ϕ (upper dashed line in Fig. 2) which fits the "data" quite well. It is convenient to choose $\tau_H = \tau_\phi$; then, the exponent in Eq. 1 is just a weighted integral over the difference between the upper and lower curves in Fig. 2. Numerical computation shows that this integral is equal to 1.71. Substituting this value and the "data" for R_{IN} into Eq. 1 gives the calculated value of the surface membrane capacity to be $S_e C_{me}$ = 2.39 nF for a 1-mm length of fiber. If it is assumed that S_e (external surface area) has been

TABLE I
RESULTS FOR SKELETAL MUSCLE FIBERS

Input parameters					Synthetic data		C_{me} calculated from Eq. 1
C_{me}	g_{me}	C_{mi}	g_{mi}	R_e	ϕ	R_{IN}	
($\mu F/cm^2$)	($\mu S/cm^2$)	($\mu F/cm^2$)	($\mu S/cm^2$)	(Ωcm)		MΩ	($\mu F/cm^2$)
1	100	1	25	100	Fig. 2; Fig. 4 *a–c*	1.88	0.95
1.5	100	1	25	100	Fig. 4 *a*	1.88	1.44
1	100	1.5	25	100	Fig. 4 *a*	1.88	0.94
1	200	1	25	100	Fig. 4 *b*	1.28	0.95
1	100	1	50	100	Fig. 4 *b*	1.24	0.95
1	100	1	25	250	Fig. 4 *c*	1.89	0.96
1	100	1	25	450	Fig. 4 *c*	1.92	0.96

The results of applying Eq. 1 to synthetic data generated by the disk model of a skeletal muscle fiber. The sixth and seventh columns show the phase angle (ϕ) of the admittance and the input resistance (R_{IN}) of a 1-mm length of fiber that is characterized by the electrical parameters in the first five columns and has no intracellular resistance. C_{me} (C_{mi}) and g_{me} (g_{mi}) are the specific capacitance and conductance of the surface (invaginated) membrane; R_e is the specific resistivity of the medium in the extracellular space (T system). When this "data" for R_{IN} and ϕ (suitably extrapolated to higher and lower frequencies) is substituted into Eq. 1, we are led to the values of C_{me} listed in the last column.

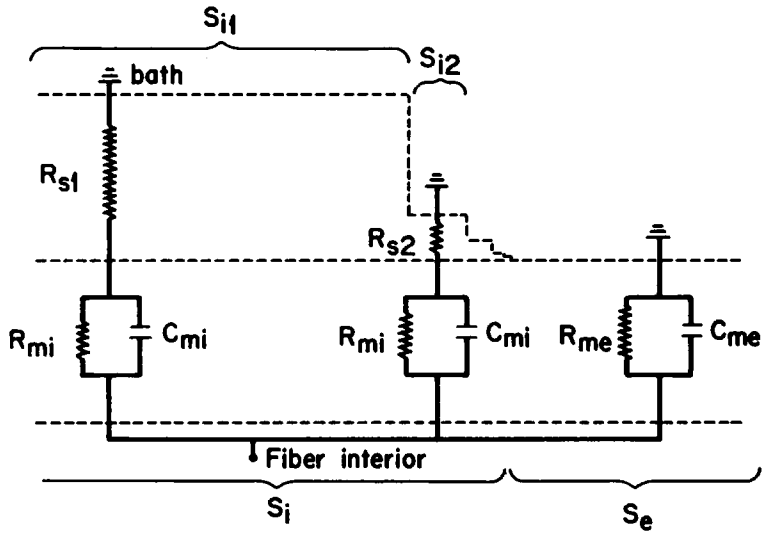

FIGURE 3 The form of the distributed circuit that is *exactly* equivalent to the disk model of a skeletal muscle fiber and the pie model of a Purkinje fiber. In both cases the surface (invaginated) membrane has total area $S_e(S_i)$ and has specific capacitance $C_{me}(C_{mi})$ and specific resistivity $R_{me}(R_{mi})$. The values of the series resistors R_{si} and distribution parameters S_{in} are given by Eq. B4 (skeletal muscle) and Eq. B9 (Purkinje fiber). Notice that only two of an infinite series of laminated membrane segments are shown explicitly.

measured correctly, $C_{me} = 0.95\ \mu F/cm^2$. This should be compared with the input value of $C_{me} = 1.00\ \mu F/cm^2$ used to generate the "data" (see Table I). Therefore, Eq. 2 has permitted the "inversion" of the synthetic data for R_{IN} and ϕ with a computational accuracy of a few percent.

Fig. 4 and Table 1 show the "data" for ϕ and R_{IN} generated by the disk model for other values of the electrical parameters. The corresponding values of C_{me} calculated with the aid of Eq. 1 are shown in the last column of Table 1. A comparison with the input values in the first column shows that this method is theoretically accurate to within a few percent. Notice that variations in g_{me}, C_{mi}, g_{mi}, and R_e result in significant changes in the synthetic data for ϕ and R_{IN}; however, these changes cancel in Eq. 1, and the calculated value of C_{me} is unaffected.

C. *Purkinje Fiber "Data"*

Eq. 1 should be valid for any geometric configuration of the extracellular space. To illustrate this, I apply it to synthetic data generated by the "pie" model of a sheep cardiac Purkinje fiber (Shoenberg et al., 1975; Hellam and Studt, 1974; Levin and Fozzard, 1981). In this case the extracellular current flows through discrete intercellular clefts instead of through a continuous disk of "smeared out" T tubules. The values of the geometric parameters of the model are taken from the morphometric work of Mobley and Page (1971) and Hellam and Studt (1974); these and other details are given in Appendix B and in Levin and Fozzard (1981). The electrical parameters of the model are the specific capacitance (C_{me}) and conductance (g_{me}) of the surface membrane, the specific capacitance (C_{mi}) and conductance (g_{mi}) of the invaginated (cleft) membrane, and the specific resistivity (R_e) of the medium in the clefts. The

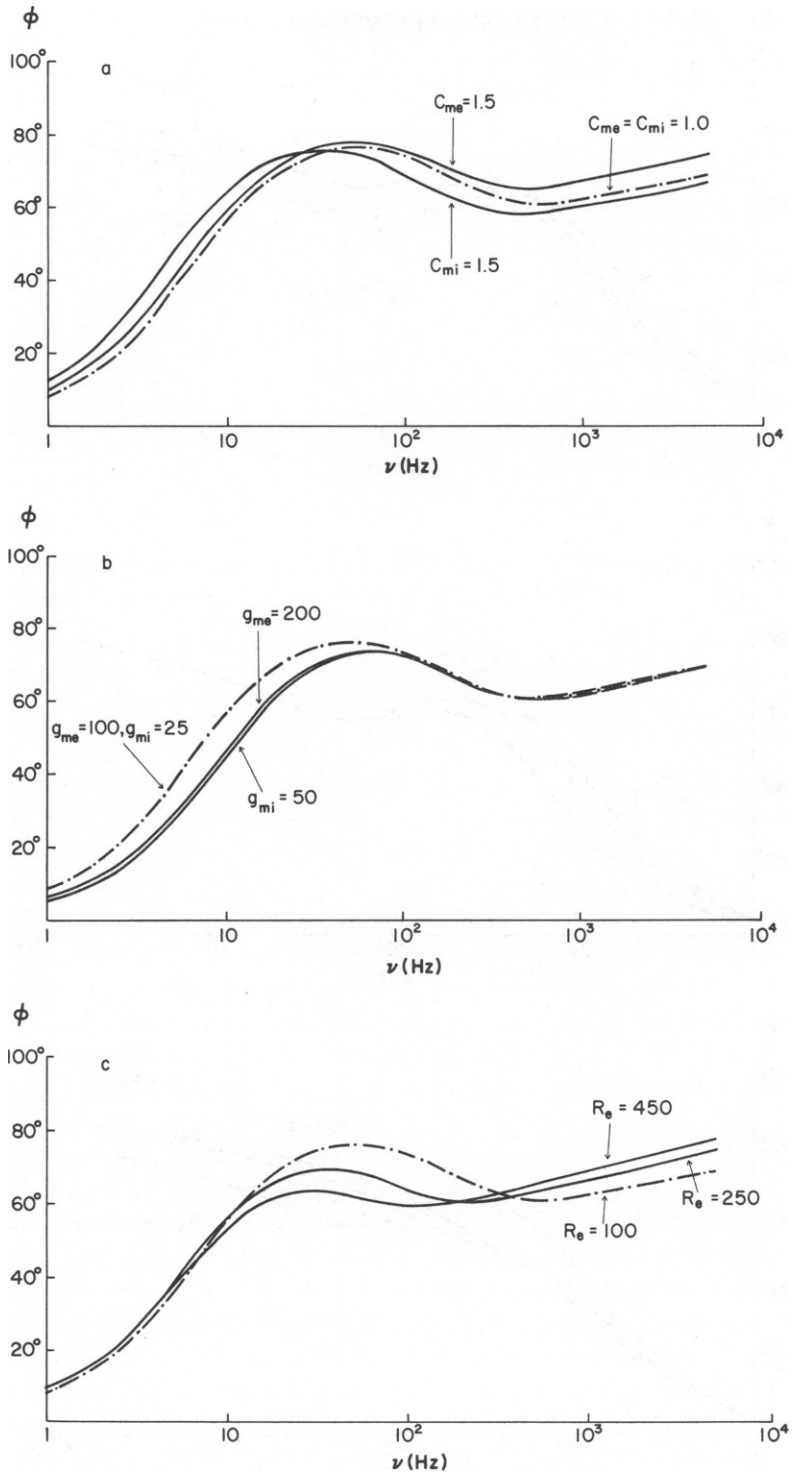

FIGURE 4 Synthetic data for the phase angle (ϕ) of the admittance of the disk model of a skeletal muscle fiber. In each panel the dot-dashed line is the same as the dot-dashed line in Fig. 2 and represents the "data" for a realistic choice of electrical parameters (given in the first line of Table I). The solid lines show how the "data" change when the value of a single electrical parameter is changed as indicated in each panel (and as listed in the remaining lines of Table I).

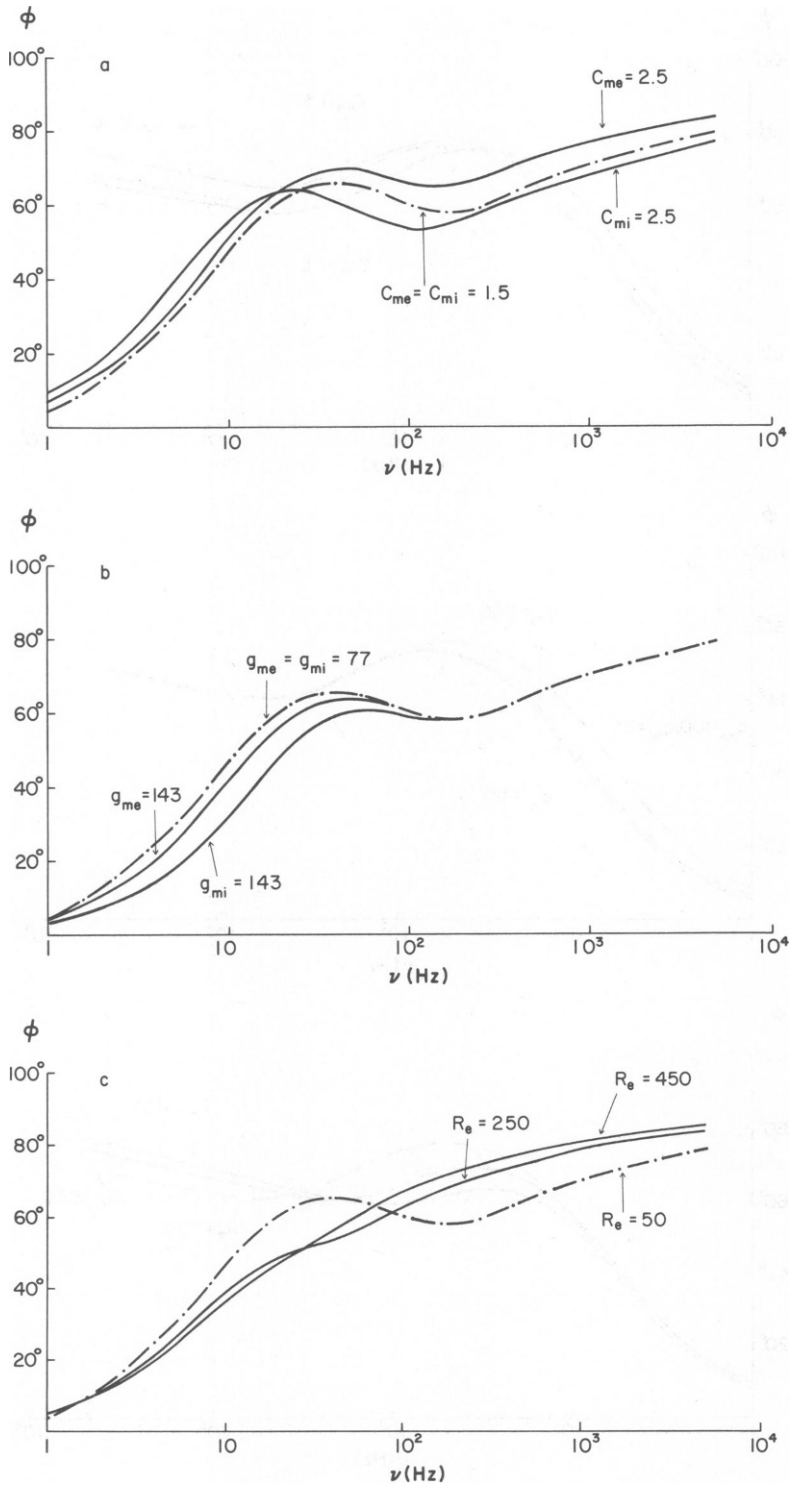

FIGURE 5 The synthetic data for the phase angle (ϕ) of the pie model of a Purkinje fiber. In each panel the dot-dashed line shows the "data" for a realistic choice of electrical parameters (given in the first line of Table II). The solid lines demonstrate how the "data" change when the value of a single electrical parameter is changed as indicated in each panel (and as listed in the remaining lines of Table II).

TABLE II
RESULTS FOR PURKINJE FIBERS

Input parameters					Synthetic data		C_{me} calculated from Eq. 1
C_{me}	g_{me}	C_{mi}	g_{mi}	R_e	ϕ	R_{IN}	
($\mu F/cm^2$)	($\mu S/cm^2$)	($\mu F/cm^2$)	($\mu S/cm^2$)	(Ωcm)		($M\Omega$)	($\mu F/cm^2$)
1.46	77	1.46	77	50	Fig. 5 *a–c*	0.48	1.42
2.5	77	1.46	77	50	Fig. 5 *a*	0.48	2.45
1.46	77	2.5	77	50	Fig. 5 *a*	0.48	1.40
1.46	143	1.46	77	50	Fig. 5 *b*	0.40	1.42
1.46	77	1.46	143	50	Fig. 5 *b*	0.30	1.42
1.46	77	1.46	77	250	Fig. 5 *c*	0.56	1.42
1.46	77	1.46	77	450	Fig. 5 *c*	0.63	1.43

The results of applying Eq. 1 to synthetic data that is generated by the pie model of a sheep cardiac Purkinje fiber. The sixth and seventh columns give the phase angle of the admittance and the input resistance of a 1-mm length of fiber that has the electrical parameters in the first five columns. C_{me} (C_{mi}) and g_{me} (g_{mi}) denote the specific capacitance and conductance of surface (invaginated) membrane; R_e stands for the specific resistivity of the medium in the extracellular (cleft) space. The last column lists the values of C_{me} deduced from this "data" for ϕ and R_{IN} with the aid of Eq. 1.

dot-dashed curve in Fig. 5a (also shown in Fig. 5 *b* and *c*) and the top line of Table II show the phase angle and R_{IN} "data" generated by a realistic choice of electrical parameters. Fig. 5 *a–c* and the remaining lines in Table II show how the "data" change when the model's electrical parameters are changed. As before, these values of R_{IN} and ϕ are treated as "data" to be substituted into Eq. 1 for the purpose of calculating C_{me}. Appendix B shows that a unit length of the pie model is also equivalent to the distributed circuit in Fig. 3, although the values of the series resistors (R_{s1}, R_{s2}, . . .) and the distribution parameters (S_{i1}, S_{i2}, . . .) are not the same as those for the skeletal muscle disk model. In effect, we are calculating C_{me} by inverting the R_{IN} and ϕ "data" from another version of the circuit in Fig. 3. It is apparent from the first and last columns of Table II that Eq. 1 faithfully reproduces the values of C_{me} used to generate the "data".

D. *Sources of Error*

The extrapolation of ϕ into the high-frequency domain may be the most serious source of experimental error in the measurement of S_eC_{me}. This can be illustrated by considering the dot-dashed curve in Fig. 2, which represents the data for a typical muscle fiber. The phase angle reaches 70° at 5,000 Hz and slowly approaches 90° at higher frequencies. If there is a 2° experimental error in ϕ at 5,000 Hz, there will be a 10% error in the integrand in Eq. 1 at that frequency. Since the integral from 5,000 Hz to ∞ contributes ~0.6 to the exponent in Eq. 1, a 10% error in the integrand will produce a multiplicative error of $e^{0.06}$ or 1.06 in Eq. 1. In short, a 2° error in the high-frequency extrapolation can result in a 6% error in the calculated value of S_eC_{me}. This is probably the major source of the discrepancy between the input and output values of C_{me} in the first and last columns of Table I. Those calculations were done with an asymptotic form which was 1.5° or 2° too low to mesh smoothly with the phase angle data at 5,000 Hz (see the slight notch between the dot-dashed curve and its dashed continuation in Fig. 2). Therefore, the high-frequency integral was too high by ~0.05, and the calculated value of C_{me} is 5% too small.

Eq. 1 is not expected to be very sensitive to systematic or random errors in the measurement of ϕ at intermediate frequencies. For example, a 1° systematic error in the measurement of ϕ from 1 to 5,000 Hz will produce a 10% error in the calculated value of S_eC_{me}. A random error of that magnitude should have a negligible effect on the calculated value of S_eC_{me}, since these errors will tend to cancel out under the integral. In any event, since the rapid acquisition of phase angle data is now possible (Mathias et al., 1979), random errors can be minimized by signal averaging.

In the examples above the integration from 0 to 1 Hz contributed a tiny amount (~0.01) to the overall integral. Therefore, the error associated with the smooth extrapolation of ϕ below 1 Hz should be neglible unless there are unsuspected phenomena in this frequency domain.

The discussion above indicates that two important types of experimental error will be encountered if Eq. 1 is used to measure the magnitude of S_eC_{me}: (*a*) erroneous extrapolation of ϕ into the high-frequency domain and (*b*) systematic errors in the measurement of ϕ at intermediate frequencies. If these errors are on the order of a degree or two, we can expect 15% accuracy in the measurement of S_eC_{me}. If the magnitude of C_{me} is needed, there will be additional error associated with the measurement of S_e. However, in many cases the magnitude of C_{me} may not be so interesting from a physiological point of view. It may be more important to measure the ratio of S_eC_{me} in the same preparation before and after an intervention. Eq. 1 should give a value for this ratio that is considerably more accurate than 15%, because the important errors in the measurement of ϕ will tend to cancel out in the ratio.

IV. DISCUSSION

The work presented in this and the following (Levin 1981) paper represents the solution of an "inverse problem": given the linear response of a syncytial tissue preparation, extract information about the *unit membrane's electrical circuit* without making assumptions about the geometry and resistivity of the extracellular space. Notice that this is not the same as the inverse problem discussed by Eisenberg and Mathias (1979) and by Adrian et al. (1974). These authors have sought to use the measured linear response (specifically, time integrals over transients) to deduce the invariant properties (e.g., "effective capacitance") of possible *electrical circuits for the whole tissue.*

The low-frequency capacity of a preparation has two components (Almers, 1978): (*a*) the infinite frequency capacity, which charges and discharges instantaneously; (*b*) capacity that fills and empties with a finite time constant. The second component may be due to dielectric charge movements with a given time constant, or it may correspond to a section of membrane that is accessed through a series resistance (e.g., extracellular space resistance). If ϕ can be measured at all frequencies, then Eq. 1 gives the infinite frequency component in terms of the input resistance of the preparation and a frequency domain integral over ϕ. In other words, in this ideal situation Eq. 1 gives the total surface membrane capacity at infinite frequency. In practice, ϕ can only be measured up to some maximum frequency, ν_M. To use Eq. 1 it is necessary to extrapolate the observed frequency dependence of ϕ into the region beyond ν_M. In this case, Eq. 1 gives the capacity of the preparation that has not been "lost" at frequency ν_M; i.e., it gives the capacity of the external membrane at infinite frequency plus any capacity that

responds with a time constant less than $1/2\pi\ \nu_M$. For example, if ν_M is 5,000 Hz, then $1/2\pi\ \nu_M \approx 1/30$ ms. Therefore, Eq. 1 will include any surface membrane capacity which may be due to very fast (<1/30 ms) dielectric charge movement processes. Eq. 1 will also include the capacity of any invaginated membrane accessed through a very small series resistance due to a very shallow or wide invagination. In the cases of skeletal muscle or Purkinje fibers, most T tubule or cleft membrane capacity will not be included, since it is accessed with a time constant of a millisecond or two.

Eq. 1 should make it possible to measure total surface capacity with an accuracy of 15%. The ratio of capacity before and after an intervention in the same preparation should be measurable to within a few percent, since most experimental errors on the right side of Eq. 1 will cancel out in a ratio. Therefore, Eq. 1 can be used to assay small changes in C_{me} or S_e induced by interventions. Theoretically, it is possible to make any intervention that leads to an electrically stable preparation. For example, one can imagine "clamping" the preparation at various holding voltages. Notice that it is not necessary to block the conductance of the internal membrane. The voltage dependence of C_{me} can then be deduced from the voltage dependence of the input resistance and phase angle of the preparation. In this way it may be possible to measure that part of C_{me} that is due to fast, saturatable dielectric charge movements (analogous to but faster than those observed by Schneider and Chandler [1973]). Interventions that change the lipid or protein composition of the external membrane may also be monitored by using Eq. 1 to measure changes in C_{me}.

Changes in S_e can also be detected by measuring the corresponding changes in R_{IN} and ϕ. For example, the external surface area of secretory epithelial cells will be seen to increase when secretory vesicles fuse with the membrane. An increase in the surface area of a multicellular preparation will be detected if extra cells become connected to the syncytium due to the formation of new gap junctions. On the other hand, an increase in the bath's osmolarity or the contraction of a muscle preparation will cause the external surface to become more wrinkled or folded. These interventions may cause wide, shallow invaginations to be converted into narrow, deep ones. The result will be a decrease in the observed value of S_e.

APPENDIX A: DERIVATION OF FORMULA FOR CAPACITY

This section contains an outline of the proof of Eq. 1; the proof is based on mathematical techniques that have been used by others in a completely different context (Omnès, 1958; Barton, 1965).

Let $y_m(p)$ be the complex admittance of the tissue preparation; p is the Laplace transform variable. At $p = i\omega = 2\pi i\nu$, y_m can be written in terms of its magnitude and phase:

$$y_m(i\omega) = |y_m(i\omega)|\, e^{i\phi(\omega)}.$$

$|y_m|$ and ϕ can be measured experimentally by driving the preparation with a sinusoidal current of frequency ν. In other words, these quantities are related to impedance locus measurements, $|y_m|$ being the inverse of the magnitude of the complex impedance and ϕ being minus the phase angle of the complex impedance of the preparation. The stability of the preparation under small steps of the voltage or current (the fifth assumption in section II) implies that $y_m(p)$ is analytic with all singularities and zeroes to the left of the imaginary axis. It is not difficult to verify this property for specific electric circuits (e.g., Figs. 1 and 3). To prove this generally, consider what happens to the preparation when the voltage is stepped from zero to V_S at $t = 0$. The Laplace-transformed voltage is V_S/p, and the

Laplace-transformed current is $y_m V_S/p$. The time dependence of the current, $J(t)$, is obtained by integrating along a contour γ, with all singularities to the left:

$$J(t) = \frac{V_S}{2\pi i}\int_\gamma dp y_m e^{pt}/p.$$

It is not difficult to see that any singularity of y_m on or to the right of the imaginary axis contributes a component to $J(t)$ that oscillates or grows indefinitely. On the other hand, any singularities of y_m to the left of the imaginary axis contribute transient components to $J(t)$. We conclude that a preparation stable to small steps in voltage has an admittance with all singularities to the left of the imaginary axis. In the same way, stability of the preparation to small current steps implies that the singularities of the complex impedance are to the left of the imaginary axis. It follows that all singularities and zeroes of y_m are to the left of the imaginary axis.

Let $H(p)$ be any "real" $[H(p)^* = H(p^*)]$ function of p whose singularities and zeroes lie to the left and that approaches p as $p \to \infty$. In essence, $H(p)$ can be the admittance of any ordinary electrical circuit that behaves capacitively at high frequencies. ϕ_H denotes the phase of H at $p = i\omega$. Define $\tilde{\Gamma}$ to be:

$$\tilde{\Gamma} = \frac{y_m}{S_e C_{me} H}. \tag{A1}$$

It follows that $\tilde{\Gamma}$ is also analytic in p with all singularities and zeroes in the left half-plane. The capacitive nature of the membranes at high frequency and the resistive nature of the extracellular medium (see the second and third assumptions in section II) guarantee that $y_m \to S_e C_{me} p$ as $p \to \infty$. It follows that $\tilde{\Gamma} \to 1$ as $p \to \infty$. If α is defined so that $p = \sqrt{\alpha}$, $\tilde{\Gamma}$ can be regarded as an analytic, nonzero function of α that has a cut along the negative real axis and which approaches 1 as $\alpha \to \infty$.

The next step in the proof requires the construction of the function Γ:

$$\Gamma = \exp\left[\frac{2}{\pi}\int_0^\infty d\omega \frac{\omega(\phi_H - \phi)}{\omega^2 + \alpha}\right]. \tag{A2}$$

It is not difficult to prove that Γ is also an analytic function of α that has a cut on the negative real axis and that approaches 1 as $\alpha \to \infty$. It follows that $\Gamma/\tilde{\Gamma}$ has the same properties. Notice that $\phi - \phi_H$ represents the phase of both Γ and $\tilde{\Gamma}$ when α is on the top lip of the cut. Therefore, $\Gamma/\tilde{\Gamma}$ is real at that point. Since y_m, H, $\tilde{\Gamma}$, and Γ are all "real" [e.g., $y_m(p)^* = y_m(p^*)$], $\Gamma/\tilde{\Gamma}$ attains the same value on both the top and bottom lips of the cut. It follows that $\Gamma/\tilde{\Gamma}$ is entire. Since $\Gamma/\tilde{\Gamma} \to 1$ as $\alpha \to \infty$, it must be identically unity everywhere; i.e., $\Gamma = \tilde{\Gamma}$. Therefore, we have proved that for all p on or to the right of the imaginary axis

$$y_m = S_e C_{me} H \Gamma, \tag{A3}$$

where

$$\Gamma(p) = \exp\left[\frac{2}{\pi}\int_0^\infty d\omega \frac{\omega(\phi_H - \phi)}{\omega^2 + p^2}\right].$$

This is a "phase representation" of the complex admittance. Eq. A3 shows that the complete behavior of the complex admittance (in particular, its magnitude) can be reconstructed from knowledge of the phase angle and $S_e C_{me}$. In this sense, measurements of the magnitude of the complex admittance are redundant if ϕ has been measured at all frequencies. The complex admittance can also be constructed from knowledge of the magnitude of the admittance at each frequency:

$$y_m = \exp\left[\frac{2p}{\pi}\int_0^\infty d\omega \frac{\ln|y_m(\omega)|}{\omega^2 + p^2}\right]. \tag{A4}$$

This "magnitude representation" is not as useful as Eq. A3, because experimental errors in the measurement of $|y_m|$ are larger than those in the measurement of ϕ. Notice that the integral generates a factor $1/p$ that cancels the factor p preceding it. For example, if $y_m(\omega)$ is equal to a constant c at all ω, the integral in Eq. A4 is just

$$\ln c \int_0^\infty \frac{d\omega}{\omega^2 + p^2} = \frac{\ln c}{p} \int_0^\infty \frac{ds}{1 + s^2} = \frac{\pi \ln c}{2p}.$$

Therefore, the right side of Eq. A4 is $e^{\ln c} = c$ as required.

A formula for $S_e C_{me}$ can be derived by setting $p = 0$ in Eq. A3 and noting that $y_m(0) = 1/R_{IN}$:

$$S_e C_{me} = \frac{1}{R_{IN} H(0) \Gamma(0)}. \tag{A5}$$

As long as ϕ_H and $H(0)$ represent the phase and zero frequency limit of a function with suitable analyticity properties, their effects will cancel exactly on the right-hand side. Eq. 1 is a special case of Eq. A5 in which $H(p)$ is chosen to be

$$H(p) = \frac{1}{\tau_H} + p,$$

where τ_H is any positive number. Eq 1 follows by substituting $\phi_H = \tan^{-1}(\tau_H \omega)$ and $H(0) = 1/\tau_H$ into Eq. A5.

APPENDIX B: MODELS OF SKELETAL MUSCLE AND PURKINJE FIBERS

The synthetic data in section III were generated by the disk model of skeletal muscle (Falk and Fatt, 1964; Adrian et al., 1969) and the pie model of a cardiac Purkinje fiber (Schoenberg et al., 1975; Hellam and Studt, 1974; Levin and Fozzard, 1981). The following is an outline of the main features of these theories.

Let $Y_e(Y_i)$ denote the specific admittance of the unit surface (invaginated) membranes. Usually, Y_e and Y_i will be taken to be the admittances of simple RC circuits:

$$\begin{aligned} Y_e &= g_{me} + C_{me} p \\ Y_i &= g_{mi} + C_{mi} p \end{aligned} \tag{B1}$$

Here, p is the Laplace transform variable, and g_{me}, $g_{mi}(C_{me}, C_{mi})$ denote the specific conductance (capacitance) of a unit membrane. S_e (S_i) will stand for the total area of surface (invaginated) membrane in a unit length of fiber. Then, the (transverse) admittance per unit length of fiber is y_m:

$$y_m = S_e Y_e + S_i Y_i F \tag{B2}$$

F is the fraction of invaginated membrane that is conducting effectively. The functional dependence of F on Y_i is determined by the geometry and resistivity of the extracellular space.

1. *Disk Model of a Skeletal Muscle Fiber*

In this model the T tubules are "smeared out" into a series of disklike extracellular spaces that are oriented transversely to the fiber axis. The form of F is found by solving the differential equations of electrical conduction for the current flow in the disk; the result is

$$F = \frac{I_1\left(\frac{a}{\lambda_T}\right)}{\left(\frac{a}{2\lambda_T}\right) I_0\left(\frac{a}{\lambda_T}\right)}, \tag{B3}$$

where

$$\lambda_T = \sqrt{\frac{\sigma\zeta}{R_e Y_i}}.$$

In the equation above, I_1 and I_0 are hyperbolic Bessel functions, a is the fiber's radius, ζ is the volume-to-surface ratio of the T system, σ is a network factor (of order ½) that accounts for various possible branching patterns of the actual T system, R_e is the specific resistivity of the medium in the T system, and Y_i is given by Eq. B1. If we assume a smooth external surface (i.e., we ignore the caveolae for simplicity), S_e is equal to $2\pi a$; S_i is given by $\pi a^2 \rho/\zeta$ where ρ is the ratio of T system volume to fiber volume. The synthetic data in section III were generated with the aid of the morphometric measurements of Mobley and Eisenberg (1975): $a = 40\mu m$, $\zeta = 0.014\ \mu m$, $\sigma = 0.32$, and $\rho = 0.0032$.

A series representation for F can be found by noting that F is analytic in Y_i except for poles

$$F = \frac{1}{S_i}\sum_{n=1}^{\infty}\frac{S_{in}}{1 + R_{sn}Y_i}, \tag{B4}$$

where

$$R_{sn} = \frac{a^2 R_e}{\alpha_n^2 \sigma\zeta},$$

$$S_{in} = \frac{4S_i}{\alpha_n^2},$$

and the α_n are the positive zeroes of the Bessel function $J_0(\alpha_n)$. It follows that the admittance of a unit length is

$$y_m = S_c Y_e + \sum_{n=1}^{\infty}\frac{S_{in}Y_i}{1 + R_{sn}Y_i}. \tag{B5}$$

Each term in the summation is the admittance of a laminated segment of invaginated membrane that has area S_{in} and that consists of a layer with admittance Y_i in series with a purely resistive layer of specific resistivity R_{sn}. Therefore, Eq. B5 shows that a unit length of the disk model behaves exactly like the terraced array of laminated segments in Fig. 3.

The synthetic data for $R_{IN} = y_m(0)^{-1}$ are obtained by evaluating Eq. B5 for various values of the electrical parameters. The data for ϕ are generated by using

$$\phi = \tan^{-1}(\tau_e\omega) + \tan^{-1}\left(\frac{S_i\tilde{F}_I}{S_e + S_i\tilde{F}_R}\right), \tag{B6}$$

where

$$\tilde{F}_R = \left(\frac{g_{mi}}{g_{me}}\right)\frac{F_R(1 + \tau_e\tau_i\omega^2) - F_I(\tau_i\omega - \tau_e\omega)}{1 + \tau_e^2\omega^2}$$

and

$$\tilde{F}_I = \left(\frac{g_{mi}}{g_{me}}\right)\frac{F_R(\tau_i\omega - \tau_e\omega) + F_I(1 + \tau_e\tau_i\omega^2)}{1 + \tau_e^2\omega^2}.$$

Here, $\tau_e(\tau_i)$ stands for $C_{me}/g_{me}(C_{mi}/g_{mi})$, the time constant of the surface (invaginated) membrane. F_R and F_I are the real and imaginary parts of F at $p = i\omega = 2\pi i\nu$ and can be obtained from Eq. B4. At high

frequency, ϕ has an asymptotic from that can be derived by substituting the large p expansion of Eq. B3 into Eq. B6; the result is

$$\phi = \frac{\pi}{2} - \frac{1}{1 + B\nu^{1/2}}, \tag{B7 a}$$

where

$$B = \frac{S_e a}{S_i}\left(\frac{\pi R_e C_{me}^2}{\sigma \zeta C_{mi}}\right)^{1/2}. \tag{B7 b}$$

2. *Pie Model of a Sheep Cardiac Purkinje Fiber*

The morphometric work of Mobley and Page (1971) and Hellam and Studt (1974) suggests that a fiber with a 100-μm diameter might be represented as the arrangement of six wedge-shaped cells with folded sides. After current leaks out through the invaginated membrane, it flows in the transverse plane through narrow meandering intercellular clefts. F is found by solving the differential equations of electrical conduction for the current flow in the extracellular space. The result is

$$F = \frac{[\cosh(L/\lambda_c) + 1]\tanh(L/2\lambda_c)}{(L/\lambda_c)\cosh(L/\lambda_c)}, \tag{B8}$$

where

$$\lambda_c = \left(\frac{w}{2R_e Y_i}\right)^{1/2}.$$

Here, L is the length (including folding) of each internal cell side, w is the width of the clefts, R_e is the specific resistivity of the cleft medium, and Y_i is given by Eq. B1. In Eq. B2 S_e is given by $2\pi a\phi_e^2$, and S_i is $12L\phi_i$, where ϕ_e and ϕ_i account for the folding of surface and invaginated membrane. In this paper we have used the geometric parameters suggested by the work of Mobley and Page (1971): L = 104 μm, w = 0.04 μm, ϕ_e = 1.4, ϕ_i = 1.9, a = 50 μm.

As in the skeletal muscle case F can be represented as a sum of poles in the complex Y_i plane:

$$F = \frac{1}{S_i}\sum_{n\text{-odd}\geq 1}\frac{S_{in}}{1 + R_{sn}Y_i}, \tag{B9}$$

where

$$R_{sn} = \frac{8L^2 R_e}{n^2\pi^2 w}$$

and

$$S_{in} = \frac{8S_i}{n^2\pi^2}.$$

It follows that y_m has the form

$$y_m = S_e Y_e + \sum_{n\text{-odd}\geq 1}\frac{S_{in}Y_i}{1 + R_{sn}Y_i}. \tag{B10}$$

Therefore, a unit length of the pie model is also equivalent to the distributed circuit in Fig. 3, although the series resistors (R_{sn}) and the distribution parameters (S_{in}) are not the same as those for the disk model.

The synthetic data for $R_{IN} = y_m(0)^{-1}$ are generated by substituting values for the electrical parameters into Eq. B10 at $p = 0$. The curves for ϕ are derived by using Eq. B6; in this case F_R and F_I denote the real and imaginary parts of Eq. B9. The asymptotic form of ϕ is found by substituting the high-frequency limit of Eq. B8 into Eq. B6. This shows that ϕ is given by Eq. B7 a with B taken to be:

$$B = \frac{L_c \phi_e^2}{\phi_i} \left(\frac{2\pi R_e C_{me}^2}{C_{mi} w} \right)^{1/2}. \tag{B11}$$

Here, L_c is the average circumferential distance (folding ignored) between cleft mouths.

The author would like to acknowledge many helpful and stimulating discussions with H. A. Fozzard and R. S. Eisenberg.

This research was supported in part by U. S. Public Health Service Program Project HL-20592.

Received for publication 8 April 1980 and in revised form 10 December 1980.

REFERENCES

Adrian R. H., W. Almers, and W. K. Chandler. 1974. Appendix: muscle membrane capacity and ionic strength. *J. Physiol. (Lond.).* 237:601

Adrian, R. H., W. K. Chandler, and A. L. Hodgkin. 1969. The kinetics of mechanical activation in frog muscle. *J. Physiol. (Lond.).* 204:207.

Adrian, R. H., W. K. Chandler, and A. L. Hodgkin. 1970. Voltage clamp experiments in striated muscle fibers. *J. Physiol. (Lond.).* 208:607.

Almers, W. 1978. Gating currents and charge movements in excitable membranes. *Rev. Physiol. Biochem. Pharmacol.* Vol. 82.

Barton, G. 1965. Dispersion Techniques in Field Theory. W. A. Benjamin, Inc., New York. 143-155.

Cole, K. S. 1972. Membranes, Ions, and Impulses. University of California Press, Berkeley. 299.

Cole, K. S., and R. H. Cole. 1941. Dispersion and absorption in dielectrics. I. *J. Chem. Phys.* 9:341.

Dwight, H. B. 1962. Tables of Integrals and Other Mathematical Data. Macmillan, Inc., New York. 30, 47, 214.

Eisenberg, R. S., V. Barcilon, and R. T. Mathias. 1979. Electrical properties of spherical syncytia. *Biophys. J.* 25:151.

Eisenberg, R. S., and E. A. Johnson. 1970. Three-dimensional electric field problems in physiology. *Prog. Biophys. Mol. Biol.* 20:1.

Eisenberg, R. S., and R. T. Mathias. 1979. Structural analysis of electrical properties. *Crit. Rev. Bioeng.* In press.

Falk, G., and P. Fatt. 1964. Linear electrical properties of striated muscle fibers observed with intracellular electrodes. *Proc. Roy. Soc. Lond. B Biol. Sci.* 160:69.

Hellam, D. C., and J. W. Studt. 1974. A core-conductor model of the cardiac Purkinje fibre based on structural analysis. *J. Physiol. (Lond.).* 243:637.

Kronig, R. de L. 1926. On the theory of dispersion of x-rays. *J. Opt. Soc. Am.* 12:547.

Levin, D. N. 1981. Unit membrane parameters of electrically syncytial tissues. *Biophys. J.* 34:147–000.

Levin, D. N., and H. A. Fozzard. 1981. A cleft model for cardiac Purkinje strands. *Biophys. J.* 33:383–408.

Mathias, R. T., R. S. Eisenberg, and R. Valdiosera. 1977. Electrical properties of frog skeletal muscle fibers interpreted with a mesh model of the tubular system. *Biophys. J.* 17:57.

Mathias, R. T., J. L. Rae, and R. S. Eisenberg. 1979. Properties of structural components of the crystalline lens. *Biophys. J.* 25:181.

Mobley, B. A., and B. Eisenberg. 1975. Sizes of components of frog skeletal muscle measured by methods of stereology. *J. Gen. Physiol.* 66:31.

Mobley, B. A., and E. Page. 1971. The surface area of sheep cardiac Purkinje fibers. *J. Physiol. (Lond.).* 220:547.

Omnès, R. 1958. On the solution of certain singular integral equations of quantum field theory. *Nuovo Cimento.* 8:316.

Peskoff, A. 1979. Electric potential in three-dimensional electrically syncytial tissues. *Bull. Math. Biol.* 41:163.

Schneider, M. F., and W. K. Chandler. 1973. Voltage dependent charge movement in skeletal muscle: a possible step in excitation-contraction coupling. *Nature (Lond.).* 242:244.

Schoenberg, M., G. Dominguez, and H. A. Fozzard. 1975. Effect of diameter on membrane capacity and conductance of sheep cardiac Purkinje fibers. *J. Gen. Physiol.* 65:441.